Fractality of the nonequilibrium stationary states of open volume-preserving systems. II. Galton boards

Felipe Barra,[1] Pierre Gaspard,[2] and Thomas Gilbert[2]

[1]*Departamento de Física, Facultad de Ciencias Físicas y Matemáticas, Universidad de Chile, Casilla, 487-3 Santiago, Chile*
[2]*Center for Nonlinear Phenomena and Complex Systems, Université Libre de Bruxelles, CP 231, Campus Plaine,*
B-1050 Brussels, Belgium

Galton boards are models of deterministic diffusion in a uniform external field, akin to driven periodic Lorentz gases, here considered in the absence of dissipation mechanism. Assuming a cylindrical geometry with axis along the direction of the external field, the two-dimensional board becomes a model for one-dimensional mass transport along the direction of the external field. This is a purely diffusive process which admits fractal nonequilibrium stationary states under flux boundary conditions. Analytical results are obtained for the statistics of multibaker maps modeling such a nonuniform diffusion process. A correspondence is established between the local phase-space statistics and their macroscopic counterparts. The fractality of the invariant state is shown to be responsible for the positiveness of the entropy production rate.

I. INTRODUCTION

Studying the statistical properties of simple mechanical models with strongly chaotic dynamics helps understanding the connection between deterministic motion at the microscopic scale and transport processes which occur at the macroscopic scales. This is of particular importance with regards to the irreversibility of thermodynamics and specifically the dynamical origins of the positiveness of entropy production [1].

Such a mechanical device was originally introduced by Galton [2] in the form of an apparatus which provides a mechanical illustration of the Gaussian spreading of independent random events. The Galton board, also known as quincunx or bean machine [3], consists of an upright board with a periodic array of pegs upon which a charge of small shots is released. The particles are let to collide on the way downward, thus displaying a seemingly erratic motion through the successive rows of pegs, until they reach the bottom of the board, where they are stopped.

Provided the actual dynamics are sufficiently chaotic and dissipative, one can idealize individual paths as Bernoulli trials, whereby every collision event results into the pellets hopping down to the right or left of the pegs with equal probabilities. The number of steps in the trials is then specified by the number of the rows of pegs in the board. Under such conditions, the heaps of shots that form at the bottom of the board are expected to be distributed according to a binomial distribution and thus approximate a normal distribution.

Though Galton's board was intended precisely as a mechanical illustration of this idealized model, the dynamics of the board are necessarily more intricate, in particular, with regards to inelasticity of the collisions between pegs and pellets and the friction exerted by the board's surface on the pellets. However if the collisions between the pellets and pegs were perfectly elastic and the board frictionless, the energy of every individual pellet would be conserved along its path. As a consequence, the kinetic energy would increase linearly with the distance separating the pellet position from

the top of the board, where one can assume it was released with a specified velocity, which, for the sake of specializing the motion to a fixed energy shell, we assume to be equal in magnitude for all pellets. Such a conservative Galton board is also referred to as idealized.

The remarkable property of conservative Galton boards is that a pellet's motion is recurrent, which is contrary to what had until recently seemed to be a widespread consensus. In other words, however far a pellet goes in the direction of the external field and consequently however large its kinetic energy becomes, it will come back to the top of the board with probability one. This property was proved by Chernov and Dolgopyat [4,5], who also showed, in accordance to previous heuristic arguments and numerical studies [6,7], that the presence of the external field affects the scaling law of positions and velocities so that a pellet's speed scales according to $v(t) \sim t^{1/3}$ and its coordinate $x(t) \sim t^{2/3}$. As described in [6], the heuristic argument posits that the parabolic motion of tracer particles in the external field induces an anisotropy between the scattering events, which can be described in terms of an effective bias that is inversely proportional to v^2. The logical consequence is that the speed grows in time as $t^{1/3}$. Chernov and Dolgopyat further found exact limit distributions for the rescaled velocity $t^{-1/3}v(t)$ and position $t^{-2/3}x(t)$.

Galton boards and related models have attracted much attention in the statistical physics community. In particular, Lorentz gases, which describe the motion of independent classical point particles in an array of fixed scattering disks, have been the subject of intensive investigations as models of diffusive transport of light tracer particles among heavier ones [8–12]. Lorentz gases have enjoyed a privileged status in the development of nonequilibrium statistical mechanics, which stems from the simplicity of its dynamics. By neglecting the recoil of heavy particles upon collision with the light tracer particles, one obtains a low-dimensional model that is amenable to a proper thermodynamical treatment while it retains important characteristics of genuine many-particle systems. This model has been studied with mathematical

rigor and, in particular, the existence of a well-defined diffusion coefficient has been proved rigorously under certain conditions [13]. Furthermore, in the last decades and in the context of molecular dynamics simulations of nonequilibrium systems [14,15], several versions of the Lorentz gas model have been considered, including the Gaussian thermostated Lorentz gas in the presence of a uniform external field [16], for which the Einstein relation between the coefficients of electrical conductivity and diffusion has been proved [17].

The reason for the initial success of the Lorentz gas was its use by Lorentz [8], elaborating on Drude's theory of electrical and thermal conduction [18,19], for the sake of deriving the Wiedemann-Franz law, which predicts the temperature dependence of the ratio between heat and electrical conductivities in metals. In this framework, the computation of the electrical conductivity assumes that the external field is weak enough that the tracer particle velocity magnitude is constant. Thus the diffusion coefficient is homogeneous and essentially given by the product of the particle's mean free path and (thermal) velocity.

In a conservative diffusive system acted upon by an external field, the situation is different in that the external field causes the acceleration of particles and induces a velocity-dependent diffusion coefficient. Nevertheless such a system bears strong analogies with the field-free diffusive case.

It is our purpose to investigate this analogy by comparing the statistical properties of Galton boards to that of periodic Lorentz gases. The latter were studied in a first paper [20], where we discussed the fractality of the nonequilibrium stationary states of open Lorentz gases under flux boundary conditions, i.e., a slab of finite extension with its two boundaries in contact with particle reservoirs with differing injection rates. Under such boundary conditions, the Lorentz gas sustains a steady current of mass which induces a constant rate of entropy production.

In [20], we established the connection between this production of entropy and the fractality of the stationary states of open Lorentz gases. In this follow-up paper, we extend these results to Galton boards and related models. In particular, we develop a discrete random-walk model that mimics the collision dynamics of Galton boards and associate to it a multibaker map with energy, similar to models introduced in [21,22]. The specificity of our model is that the transition rates vary with the sites' indices, reflecting the property of the conservative Galton board that deflection of tracers by the external field is more likely to occur when their kinetic energies are small in comparison to their potential energies. We derive the analytic expression of the nonequilibrium stationary states of this multibaker map and show that its cumulative measures are characterized by nowhere differentiable continuous functions similar to the Takagi function of the nonequilibrium stationary state of the usual multibaker map [23]. This allows us to compute the entropy associated to such nonequilibrium stationary states and thus obtain an analytic derivation of the rate of entropy production, which, within our formalism, finds its origin in the fractality of the nonequilibrium stationary state, in agreement with the results presented in [20] for the field-free case.

The paper is organized as follows. Galton boards are presented in Sec. II. The connection to the phenomenology of diffusion in an external field, described in Sec. II A, is established for both closed and open systems, whose statistical properties are considered in Sec. II B. These properties are then studied numerically, first under equilibrium setting in Sec. II C, and then under nonequilibrium setting in Sec. II D, where we demonstrate the fractality of the invariant measure. In Sec. III, we introduce the forced multibaker map, which mimics the collision dynamics of the Galton board and analyze its statistics in Sec. III A. The entropy production rate of the nonequilibrium stationary state is computed in Sec. III B. We end with conclusions in Sec. IV. In Appendix A we discuss the occurrence of elliptic islands in the Galton board's dynamics, i.e., the stabilization of periodic orbits, and provide conditions under which we can assume the system to be fully hyperbolic. Appendixes B and C provide detailed derivations of the nonequilibrium stationary state of the forced multibaker map and coarse-grained entropies.

II. GALTON BOARD

The Galton board is similar to a periodic Lorentz gas in a uniform field. We consider a two-dimensional cylinder of length $L=Nl$ and height $\sqrt{3}l$, with disks $\mathbb{D}_n$, $0 \leq n \leq 2N$, of radii σ, $\sqrt{3}/4 < \sigma/l < 1/2$, placed on a hexagonal lattice structure. The centers of the disks take positions

$$(x_n, y_n) = \begin{cases} (nl/2, 0), & n \text{ odd} \\ (nl/2, \pm\sqrt{3}l/2), & n \text{ even,} \end{cases} \quad (1)$$

where we identify the disks $y = \pm\sqrt{3}l/2$.

Notice here that, contrary to the convention used in Ref. [20], n takes only positive values. As will be made clear in the sequel, this choice reflects the impossibility for trajectories to travel beyond the barrier defined by the zero kinetic-energy line, perpendicular to the axis of the cylinder.

Following conventions similar to [20], the cylindrical region around disk $\mathbb{D}_n$ is defined as

$$\mathbb{I}_n = \{(x,y) | (n-1/2)l/2 \leq x \leq (n+1/2)l/2\}. \quad (2)$$

Thus the interior of the cylinder, where particles propagate freely is made up of the union $\cup_{n=-N}^{N} \mathbb{I}_n \backslash \mathbb{D}_n$.

The associated phase space, defined on a constant energy shell, is $\mathbb{C} = \cup_{n=-N}^{N} \mathbb{C}_n$, where $\mathbb{C}_n = \mathbb{S}^1 \otimes [\mathbb{I}_n \backslash \mathbb{D}_n]$ and the unit circle $\mathbb{S}^1$ represents all possible velocity directions. Particles are reflected with elastic collision rules on the border $\partial\mathbb{C}$, except at the external borders, corresponding to $x=0, L$, where they get absorbed. Points in phase space are denoted by $\Gamma = (x, y, v_x, v_y)$ and trajectories by $\Phi^t\Gamma$, where Φ^t is the flow associated to the dynamics of the Galton board.

The collision map, which operates on $\partial\mathbb{C}$, is the natural reduction of the flow Φ^t to a discretized-time process. Given that the energy E is fixed, the collision map operates on a two-dimensional surface, which, when the collision takes place on disk n, is conveniently parametrized by the Birkhoff coordinates (ϕ_n, ξ_n), where ϕ_n specifies a generalized angle variable along the border of disk n, to be determined in Sec. II C, and ξ_n is the sinus of the angle that the particle velocity makes with respect to the outgoing normal to the disk after the collision.
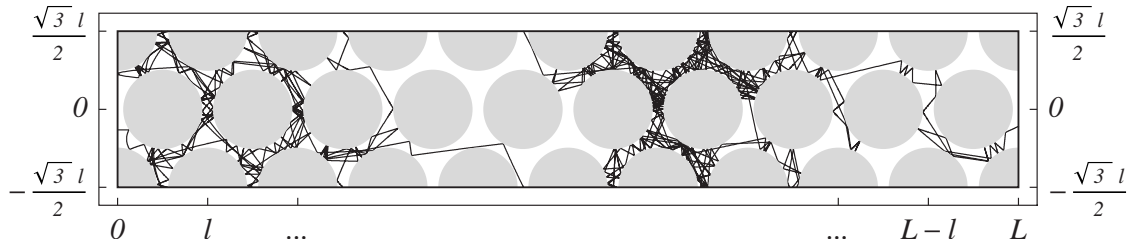
FIG. 1. Cylindrical Galton board with a nonvanishing external field and the energy $E=0$. A trajectory is released at zero velocity at $x=0$ and falls along the external field until it collides a first time with a disk. It then wanders around, coming back close to $x=0$ once, after which it moves further along the channel until it reaches the border at $x=L$. To compute the successive collision events, the numerical integration scheme uses an exact quartic equation solver based on the Galois formula [24].

The external field is uniform and directed along the positive x direction so that particles accelerate as they move along the axis of the channel, in the direction of the external field. There is no dissipative mechanism and energy is conserved along the Galton board trajectories.

In this system, as opposed to typical billiards, the energy, denoted E, can be both kinetic and potential. As the particle moves along the direction of the channel axis, it loses potential energy and gains kinetic energy, according to the energy conservation $E = (v_x^2 + v_y^2)/2 - \epsilon x$, where ϵ denotes the amplitude of the external field. Conversely, the particle loses kinetic energy and gains potential energy as it moves in the direction opposite to the external field.

Assuming $E \geq 0$, the boundaries of the system are placed at $x=0$ and $x=L$, reflecting the impossibility for a trajectory to gain potential energy beyond the zero kinetic-energy level. When $E=0$, trajectories turn around at $x \geq 0$ when the x component of the velocity annihilates, whereas when $E > 0$, depending on the choice of boundary conditions, particles can be either reflected or absorbed when they reach $x=0$.

The trajectory between two successive elastic collisions with the disks is now parabolic, according to $x(t) = x(0) + v_x(0)t + \epsilon t^2/2$, whereas the vertical motion is uniform $y(t) = y(0) + v_y(0)t$. The amplitude of the external field ϵ can be set to unity by an appropriate rescaling of the momenta and time variable: $v \to v/\sqrt{\epsilon}$ and $t \to t\sqrt{\epsilon}$. Correspondingly, the energy has the units of length.

We can thus write the velocity amplitude as a function of the x coordinate,

$$v(x) = \sqrt{2(E+x)}. \tag{3}$$

In particular, the velocity amplitude at $x=0$ is $v(0) = \sqrt{2E}$. We will assume that the energy takes half-integer values of the cell widths l so that the kinetic energy takes half-integer values at the horizontal positions of the disks along the channel, i.e., at xs which are half-integer multiples of l.

The system is shown in Fig. 1 with absorbing boundary conditions at $x=0$ and L. Note that trajectories are seen to bend along the field only so long as the velocity is small enough that the action of the field is noticeable. Otherwise the trajectory looks much like that of the Lorentz channel in the absence of external field. The time scales are however different.

A. Phenomenology

One often reads in the literature that the Galton boards or equivalently the periodic Lorentz gases in a uniform external field do not have a stationary state. This is however a confusing statement since the existence of the stationary state has nothing to do with the presence of the external field. Rather, it is a matter of boundary conditions.

Just as with the usual Lorentz gas, when an external forcing is turned on, a stationary state is reached so long as one specifies the boundary conditions. The reason for much of the confusion associated to this problem is, according to our understanding, that one cannot consider periodic boundary conditions along the direction of the field since they would violate the conservation of energy. One can however consider both reflecting and absorbing boundary conditions for the extended system. The nature of the stationary state, whether equilibrium or nonequilibrium, depends on the choice of boundary conditions.

A phenomenological diffusion equation can be obtained for the motion along the axis of the cylindrical channel, which corresponds to the direction of the external field.

In the presence of an external field, the diffusion process is *a priori* biased so that the Fokker-Planck equation of diffusion reads

$$\partial_t \mathcal{P}(X,t) = \partial_X[\mathcal{D}(X)\partial_X \mathcal{P}(X,t) + \mathcal{M}(X)\mathcal{P}(X,t)]. \tag{4}$$

Here X denotes a macroscopic position, associated to the projection along the axis direction of a given phase-space region $\mathbb{I}_n$ of the Galton board, taken in the continuum limit.

According to Einstein's argument, the diffusion coefficient $\mathcal{D}(X)$ is connected to the mobility coefficient $\mathcal{M}(X)$ by the condition that Eq. (4) admits the equilibrium state $\mathcal{P}_{eq}(X)$ as a solution which annihilates the mean current:

$$\mathcal{D}(X)\partial_X \mathcal{P}_{eq}(X) + \mathcal{M}(X)\mathcal{P}_{eq}(X) = 0. \tag{5}$$

At the microscopic level, letting Γ denote a phase point in $2d$ dimensions with velocity amplitude v and position x with respect to the direction of the external field, the equilibrium state is the microcanonical state, i.e.,

$$\rho_{eq}(\Gamma) \propto \delta\left(E - \frac{v^2}{2} + x\right). \tag{6}$$

Integrating this equilibrium phase-space density over cells $\mathbb{C}_n$ and taking the continuum limit $l \to 0$ and $n \to \infty$ with the

macroscopic position variable $X=nl/2$ fixed, we obtain the macroscopic equilibrium density $\mathcal{P}_{\mathrm{eq}}(X)$,

$$\mathcal{P}_{\mathrm{eq}}(X)dX = \lim_{\substack{l \to 0 \\ n \to \infty}} \int_{C_n} d\Gamma \rho_{\mathrm{eq}}(\Gamma),$$

$$\propto \lim_{\substack{l \to 0 \\ n \to \infty}} \int_{C_n} d\Gamma \delta\left(E - \frac{v^2}{2} + x\right),$$

$$\propto \lim_{l \to 0} l \int dv v^{d-1} \delta\left(E - \frac{v^2}{2} + X\right). \quad (7)$$

Identifying the length increments $dX=l$, and carrying out the velocity integration, we arrive to the expression of the equilibrium density

$$\mathcal{P}_{\mathrm{eq}}(X) = \mathcal{N}[2(E+X)]^{(d-2)/2}, \quad (8)$$

where $\mathcal{N}$ is a normalization factor. Inserting this expression into Eq. (5), we obtain the relation between the mobility and diffusion coefficients,

$$\mathcal{M}(X) = -\frac{d-2}{2}\frac{\mathcal{D}(X)}{E+X}. \quad (9)$$

The diffusion coefficient, on the other hand, is proportional to the magnitude of the position-dependent velocity, $V(X) = \sqrt{2(E+X)}$. This is a transposition of the corresponding result for the usual field-free periodic Lorentz gas, where the tracer's velocity has constant magnitude. In the Galton board, given an energy E identical for all the tracer particles, the velocities $V(0)=\sqrt{2E}$ at $X=0$ are identical for all particles, growing with $X>0$, due to the uniform force of unit amplitude acting along that direction. We can therefore write

$$\mathcal{D}(X) = \mathcal{D}_0 \sqrt{1 + \frac{X}{E}}. \quad (10)$$

Notice the normalization so chosen that the diffusion coefficient at $X=0$ reduces to $\mathcal{D}_0$. Equation (10) can be thought of as a transposition of the argument by Machta and Zwanzig [25] who provided an analytical expression of the diffusion coefficient for the periodic Lorentz gas based upon a random-walk approximation. This approximation indeed carries over to the Galton board. Provided energy is conserved, the velocity of a tracer particle increases as it moves along the direction of the external field. Thus, provided the periodic cells have sizes small enough that velocities remain approximately constant within each cell, the Machta-Zwanzig argument tells us that the diffusion coefficient is simply multiplied by a factor which accounts for the position-dependent velocity, hence expression (10).

Plugging Eq. (10) into Eq. (9), we obtain the expression of the mobility

$$\mathcal{M}(X) = -\frac{d-2}{2}\frac{\mathcal{D}_0}{E\sqrt{1+\frac{X}{E}}}. \quad (11)$$

Remarkably, the mobility coefficient vanishes for a two-dimensional billiard. In this case, the Fokker-Planck Eq. (4) therefore simplifies to

$$\partial_t \mathcal{P}(X,t) = \partial_X[\mathcal{D}(X)\partial_X \mathcal{P}(X,t)]. \quad (12)$$

An equivalent equation was derived by Chernov and Dolgopyat in [4]. This is a diffusive equation *without* a drift and describes the recurrent motion of the two-dimensional Galton board trajectory at the macroscopic scale. In contrast, we notice that the Fokker-Planck Eq. (4) associated to a three-dimensional version of the conservative Galton board has a nonvanishing mobility coefficient [Eq. (11)] and therefore retains a drift term.

In the sequel we will assume $E>0$ so as to avoid the singularities that come with zero velocity trajectories.

We notice, on the one hand, that reflection at the boundaries (RBC) induces an equilibrium state of Eq. (12) with constant density,

$$\mathcal{P}(X) = 1, \quad (\text{RBC}). \quad (13)$$

Flux boundary conditions (FBC), on the other hand, viz.

$$\begin{aligned} \mathcal{P}(0) &\equiv \mathcal{P}_- \\ \mathcal{P}(L) &\equiv \mathcal{P}_+, \end{aligned} \quad (14)$$

admit the stationary state

$$\mathcal{P}(X) = \mathcal{P}_- + (\mathcal{P}_+ - \mathcal{P}_-)\frac{\sqrt{E+X}-\sqrt{E}}{\sqrt{E+L}-\sqrt{E}}. \quad (15)$$

Given rates $\mathcal{P}_- \neq \mathcal{P}_+$, the current associated to the nonequilibrium stationary state is constant and, according to Fick's law, equal to

$$\begin{aligned} \mathcal{J} &= -\mathcal{D}(X)\partial_X \mathcal{P}(X), \\ &= -\frac{\mathcal{D}_0}{2E}\frac{\mathcal{P}_+ - \mathcal{P}_-}{\sqrt{1+L/E}-1}. \end{aligned} \quad (16)$$

The corresponding local rate of entropy production is given according to the usual formula by the product of the mass current [Eq. (16)] and the associated thermodynamic force [26],

$$\frac{d_{\mathrm{i}}\mathcal{S}(X)}{dt} = \mathcal{D}(X)\frac{[\partial_X \mathcal{P}(X)]^2}{\mathcal{P}(X)}. \quad (17)$$

B. Discretized process

The deterministic models we consider are to be analyzed in terms of return maps, which involves a discretization of both time and length scales. We consider this problem in some detail as it will be useful for the sake of defining a discrete process associated to the Galton board.

Let the discretized time and length scales be determined according to $t=k\tau$ and $X=nl$. Collision rates are proportional to the velocity, which brings in a factor $\sqrt{1+nl/E}$ after we time discretize Eq. (12),

$$\frac{1}{\tau}\sqrt{1+\frac{nl}{E}}[\mathcal{P}(nl,k\tau+\tau)-\mathcal{P}(nl,k\tau)]$$

$$=\frac{1}{l^2}\{\mathcal{D}(nl+l/2)\mathcal{P}(nl+l,k\tau)+\mathcal{D}(nl-l/2)\mathcal{P}(nl-l,k\tau)$$

$$-[\mathcal{D}(nl+l/2)+\mathcal{D}(nl-l/2)]\mathcal{P}(nl,k\tau)\}. \quad (18)$$

We let

$$\mu_n(k)\equiv\sqrt{1+\frac{nl}{E}}\mathcal{P}(nl,k\tau) \quad (19)$$

be the collision frequency on the Poincaré surface at position $X=nl$ and introduce a diffusion coefficient associated to the discrete process,

$$D(n)\equiv\frac{\tau}{l^2}\mathcal{D}(nl). \quad (20)$$

It is convenient to set $E\equiv(2n_0+1)l/2$ for some positive integer n_0.

Equation (18) thus transposes to the evolution

$$\mu_n(k+1)=\left[1-\frac{D(n+1/2)}{\sqrt{1+\frac{2n}{2n_0+1}}}-\frac{D(n-1/2)}{\sqrt{1+\frac{2n}{2n_0+1}}}\right]\mu_n(k)$$

$$+\frac{D(n+1/2)}{\sqrt{1+\frac{2(n+1)}{2n_0+1}}}\mu_{n+1}(k)+\frac{D(n-1/2)}{\sqrt{1+\frac{2(n-1)}{2n_0+1}}}\mu_{n-1}(k). \quad (21)$$

Written under the form

$$\mu_n(k+1)=s_{n-1}^+\mu_{n-1}(k)+s_n^0\mu_n(k)+s_{n+1}^-\mu_{n+1}(k), \quad (22)$$

Eq. (21) is seen to be the Frobenius-Perron equation of the Markov process

$$n\rightarrow\begin{cases}n-1, & s_n^-\\n, & \text{with probability } s_n^0 \\ n+1, & s_n^+.\end{cases} \quad (23)$$

As opposed to a symmetric random walk, the probabilities s_n^-, s_n^0, and s_n^+ are asymmetric and depend on the site index,

$$s_n^-=\frac{D(n-1/2)}{\sqrt{1+\frac{2n}{2n_0+1}}},$$

$$s_n^+=\frac{D(n+1/2)}{\sqrt{1+\frac{2n}{2n_0+1}}},$$

$$s_n^0=1-s_n^--s_n^+. \quad (24)$$

In these expressions, n is assumed to be a positive integer, $0\leq n\leq N$. From Eq. (10), the diffusion coefficient may be written $D(n)=D_0\sqrt{1+\frac{2n}{2n_0+1}}$, where $D_0=\tau/l^2\mathcal{D}_0$, from which it follows that

$$s_n^{\pm}=D_0\sqrt{1\pm\frac{1}{2(n_0+n)+1}}. \quad (25)$$

It is straightforward to check that the stationary state of Eq. (22) is independent of D_0 and can be written under the form

$$\mu_n\equiv\lim_{k\rightarrow\infty}\mu_n(k)=\sqrt{\frac{2(n_0+n)+1}{2n_0+1}}P_n, \quad (26)$$

where P_n is the discretized stationary state of the Fokker-Planck Eq. (12),

$$P_n[\sqrt{n_0+n+1}+\sqrt{n_0+n}]=P_{n+1}\sqrt{n_0+n+1}+P_{n-1}\sqrt{n_0+n}. \quad (27)$$

We note that the latter equation implies that $\sqrt{n_0+n}$ $(P_n-P_{n-1})\equiv\alpha$ is constant. We can therefore write

$$P_n=P_{n-1}+\frac{\alpha}{\sqrt{n_0+n}}$$

$$=P_0+\alpha\sum_{i=0}^{n}(n_0+i)^{-1/2}$$

$$=P_0+\alpha(H_{n+n_0}^{1/2}-H_{n_0}^{1/2}), \quad (28)$$

where $H_{n+n_0}^{1/2}$ denotes the Harmonic number, $H_n^{1/2}=\sum_{j=1}^n j^{-1/2}$ [27]. Letting $n=N$ in Eq. (28), $Nl=L$, and writing the boundary conditions $P_0\equiv P_-$ and $P_N\equiv P_+$, we obtain the expression of α, $\alpha=(P_+-P_-)/(H_{N+n_0}^{1/2}-H_{n_0}^{1/2})$. Therefore P_n can be expressed as

$$P_n=P_-+(P_+-P_-)\frac{H_{n+n_0}^{1/2}-H_{n_0}^{1/2}}{H_{N+n_0}^{1/2}-H_{n_0}^{1/2}}. \quad (29)$$

The connection to the continuous case and, in particular, to Eq. (15) is now straightforward. Indeed, the ratio of differences of Harmonic functions become integrals when $l\rightarrow 0$

$$\frac{H_{n+n_0}^{1/2}-H_{n_0}^{1/2}}{H_{N+n_0}^{1/2}-H_{n_0}^{1/2}}=\frac{\frac{l}{\sqrt{E+l/2}}+\frac{l}{\sqrt{E+3l/2}}+\ldots+\frac{l}{\sqrt{E+l/2+nl}}}{\frac{l}{\sqrt{E+l/2}}+\frac{l}{\sqrt{E+3l/2}}+\ldots+\frac{l}{\sqrt{E+l/2+Nl}}}$$

$$\rightarrow\frac{\int_E^{E+X}dx/\sqrt{x}}{\int_E^{E+L}dx/\sqrt{x}}$$

$$=\frac{\sqrt{E+X}-\sqrt{E}}{\sqrt{E+L}-\sqrt{E}}, \quad (30)$$

where the limit assumes $l\rightarrow 0$ with E constant and thus $n_0\gg 1$. In this case we have $P_n\rightarrow\mathcal{P}(X=nl)$.

C. Equilibrium Galton board

We now turn to the stationary states of Galton boards whether equilibrium or nonequilibrium. Prior to doing so, however, we note that, contrary to the periodic Lorentz gas which has strong hyperbolic properties, Galton boards can
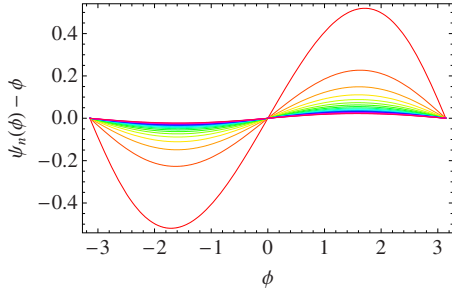
FIG. 2. (Color online) Difference between the generalized angle coordinate $\psi_n(\phi)$ and ϕ, here computed for $\sigma=0.44l$, $n_0=0$, and $n=1,\ldots,20$. Larger differences occur at smaller n, where the effect of the external field is most noticeable.

have elliptic periodic orbits. The occurrence of such orbits is discussed in Appendix A. Such elliptic islands will not be of concern to us as they can easily be suppressed by taking the energy E to be large enough. We will therefore assume in the sequel that the system is fully hyperbolic.

It is perhaps not widely appreciated that one can obtain an equilibrium state consistent with the presence of the external field. The reason for this is actually quite simple. Liouville's theorem implies the conservation of the volume measure,

$$d\Gamma = dx\,dy\,dv_x\,dv_y$$
$$= v\,dE\,dt\,d\phi\,d\xi, \qquad (31)$$

where ϕ and ξ are defined to be the angle along the disk and sinus of the outgoing velocity angle measured with respect to the normal to the disk.

We remark that because of the factor v that multiplies the volume measure in Eq. (31), the pair (ϕ,ξ) are not canonical variables. Indeed the position along the cylinder axis varies with the angle coordinate ϕ so that the velocity v depends on ϕ. The appropriate generalized angle variable conjugated to ξ can be determined accordingly [28].

Introducing the index n, referring to the nth disk, whose center has position $x=(n-1)l/2$ along the cylinder axis, the velocity at angle ϕ along disk n is

$$v_n(\phi) = \sqrt{2[E + (n-1)l/2 + \sigma\cos\phi]}$$
$$= \sqrt{(n_0+n)l + 2\sigma\cos\phi}. \qquad (32)$$

The canonical coordinate conjugated to ξ is therefore ψ_n, such that $d\psi_n = v_n(\phi)d\phi$,

$$\psi_n(\phi) = 2\pi\frac{\int_0^\phi v_n(\phi)d\phi}{\int_0^{2\pi} v_n(\phi)d\phi}$$
$$= \pi\frac{E(\frac{\phi}{2},2\frac{2\sigma}{(n+n_0)l+2\sigma})}{E(2\frac{2\sigma}{(n+n_0)l+2\sigma})}, \qquad (33)$$

where E denotes the elliptic integral of the second kind, $E(\phi,x)=\int_0^{\phi/2}\sqrt{1-x\sin^2\theta}\,d\theta$, and $E(x)=E(\pi/2,x)$ is the complete elliptic integral. As seen in Fig. 2, the difference between ψ_n and ϕ decreases rapidly as nl increases. Note that σ is assumed to scale with l so that ψ_n does not actually depend on l.

Let us consider a closed Galton board of length $L=Nl$ ($2N+1$ disks), with reflecting boundaries at $x=0$ and $x=L$. This is an equilibrium system. More precisely the invariant density associated to each disk is uniform, as verified in Fig. 3. The distinctive feature however is that the time scale changes with the disk index n, $\tau(n)\sim 1/v_n$. Thus particles move faster with increasing n, but correspondingly they make more collisions so that their distribution is uniform in time.

From the average count of collision events of disk n, we obtain the collision frequency, which, when multiplied by the local time scale (this amounts to dividing it by the velocity v_n evaluated at the center of cell n) yields the average density $P_n \sim \mathcal{P}[X_n=(n-1)l/2]$. This quantity, shown in Fig. 4, is indeed found to be almost constant, thus confirming our reasoning.

D. Nonequilibrium Galton board

A nonequilibrium stationary state of the Galton board can be achieved much in the same way as with the open Lorentz gas studied in [20] by assuming that a flux of trajectories is continuously flowing through the boundaries which are let in contact with stochastic particle reservoirs at $x=0$ and $x=L$,

$$\rho(\Gamma,t)|_{x=0,L} = \delta\left(E+x-\frac{v_x^2+v_y^2}{2}\right)\rho_\pm. \qquad (34)$$

In analogy to the field-free case [29], we denote by Γ_E the three-dimensional phase-space coordinates on the constant energy surface, $\Gamma_E=(x,y,\varphi)$, and write the invariant solution of the Liouville equation compatible with boundary conditions (34), for almost every phase point Γ_E, as
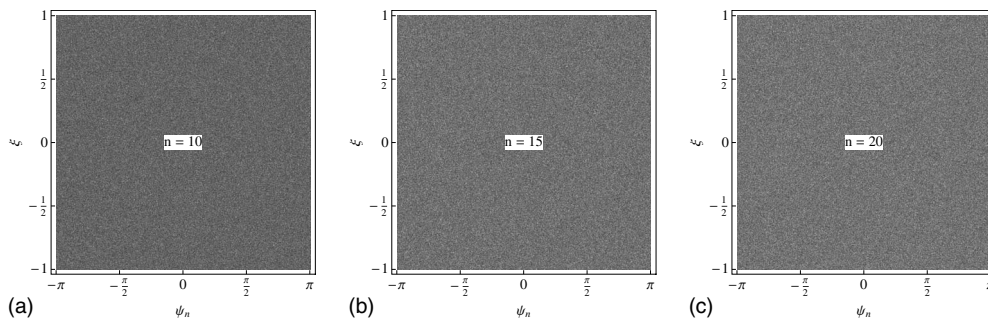

FIG. 3. Invariant density associated to a closed Galton board of size $L=10l$, with reflection at the boundaries $x=0$ and $x=10l$ and energy $E=l/2$. This is an equilibrium system as reflected by the uniformity of the phase portraits.
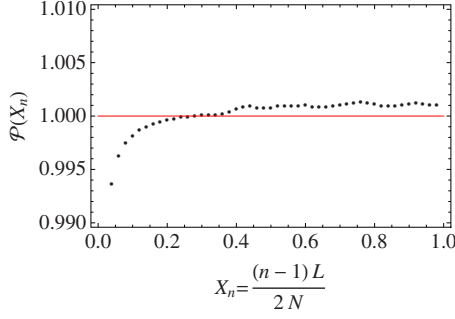
FIG. 4. (Color online) Equilibrium stationary density of the closed Galton board obtained for a channel of length $L=1$, with $2N+1$ disks, $N=25$. The solid line is the constant equilibrium density $\mathcal{P}(X)=1$.

$$\rho(\Gamma_E) = \rho_- + \frac{\rho_+ - \rho_-}{\sqrt{2(E+L)} - \sqrt{2E}}$$
$$\times \left[v(\Gamma_E) - \sqrt{2E} + \int_0^{-T(\Gamma_E)} dt \dot{v}(\Phi^t \Gamma_E) \right]. \quad (35)$$

We note that there are *a priori* infinitely many possible alternatives to this equation, compatible with boundary conditions (34). However form (35) is the only one whose regular part yields a contribution consistent with the macroscopic limit [Eq. (15)]. As described below, the validity of this comparison is checked numerically. It is also important to notice that the zero-field limit of Eq. (35) is the invariant density of the periodic Lorentz gas, as described in [20].

Thus $\rho(\Gamma_E)$ is written in terms of the change in velocity amplitude, given by $v(\Gamma_E) = \sqrt{2[E+x(\Gamma_E)]}$ at the corresponding horizontal position $x(\Gamma_E)$, with components $v_x(\Gamma_E) = v(\Gamma_E)\cos\varphi$ and $v_y(\Gamma_E) = v(\Gamma_E)\sin\varphi$. The time-derivative $\dot{v}(\Gamma_E) = \dot{x}(\Gamma_E)/v(\Gamma_E)$, and provided the change in velocity between successive collisions is small, we can write $\int_0^{\tau} \dot{v}(\Phi^t \Gamma_E) dt \simeq [x(\Phi^{\tau} \Gamma_E) - x(\Gamma_E)]/v(\Gamma_E)$. Hence, denoting by τ_k the time separating the $(k-1)$th and kth collisions and by $t_k = \sum_{j=1}^k \tau_j$ the time elapsed after k collisions, we have

$$\rho(\Gamma_E) \simeq \rho_- + \frac{\rho_+ - \rho_-}{\sqrt{2(E+L)} - \sqrt{2E}} \left[v(\Gamma_E) - \sqrt{2E} \right.$$
$$\left. + \sum_{k=1}^{K(\Gamma_E)} \frac{x(\Phi^{-t_k}\Gamma_E) - x(\Phi^{-t_{k-1}}\Gamma_E)}{v(\Phi^{-t_k}\Gamma_E)} \right]. \quad (36)$$

This approximation becomes exact when the number of cells in the system is let to infinity, in which case $K(\Gamma_E)$, the number of collisions for the trajectory to reach the boundaries becomes infinite. Therefore the invariant state is

$$\rho(\Gamma_E) = \rho_- + \frac{\rho_+ - \rho_-}{\sqrt{2(E+L)} - \sqrt{2E}} \left[v(\Gamma_E) - \sqrt{2E} \right.$$
$$\left. + \sum_{k=1}^{\infty} \frac{x(\Phi^{-t_k}\Gamma_E) - x(\Phi^{-t_{k-1}}\Gamma_E)}{v(\Phi^{-t_k}\Gamma_E)} \right] \quad (37)$$

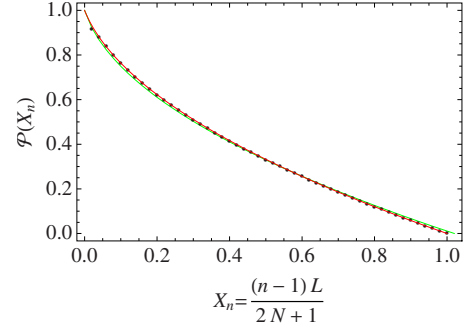so that the fluctuating part of the invariant density becomes

FIG. 5. (Color online) Nonequilibrium stationary density of the Galton board obtained for a channel of length $L=1$, with 51 disks ($N=25$). Two solid lines are shown which are barely distinguishable, corresponding to Eq. (15) (red) and Eq. (29) (green) with $E=l/2$ and thus $n_0=0$.

singular. This is analogous to the field-free case discussed in [20].

We compute this quantity numerically from the statistics of the Birkhoff map of the Galton board, using a cylindrical Galton board similar to that shown in Fig. 1, with external forcing of unit magnitude in the direction of the cylinder axis, letting the particles have energy $E=1/2$. The particles are thus injected at $x=0$ with unit velocity at random angles and subsequently absorbed upon their first passage to either $x=0$ or $x=L$.

The computation of the collision frequency at disk n, averaged over the phase-space coordinates yields the quantity μ_n [Eq. (26)], which, after dividing by the modulus of the velocity at that site, is converted to P_n, the stationary solution of the Fokker-Planck Eq. (12). Here, we have

$$\mathcal{P}(X_n) = \frac{1}{l} \int_{\mathbb{C}_n} d\Gamma \rho(\Gamma),$$
$$= \mathcal{P}_- + (\mathcal{P}_+ - \mathcal{P}_-) \frac{\sqrt{(E+X_n)} - \sqrt{E}}{\sqrt{(E+L)} - \sqrt{E}}. \quad (38)$$

The results of this computation are presented in Fig. 5 and compared to Eqs. (15) and (29). The agreement with both discrete and continuous solutions is excellent.

The histograms displayed in Fig. 6 show the fluctuating part of the invariant phase-space density computed in terms of the Birkhoff coordinates (ψ_n, ξ) [Eq. (33)]. The fractality of these graphs is much like that of the graphs of the open Lorentz gas, see [20]. The differences are indeed too tenuous to tell. As with the closed Galton board though, the distinctive feature is that the collision rates increase with the cell index with the amplitude of the velocity.

To further analyze the fractality of the stationary state of the nonequilibrium Galton board and its relation to the phenomenological entropy production [Eq. (17)], we introduce in the next section an analytically tractable model, which generalizes the multibaker map associated to a field-free symmetric diffusion process, so as to account for the acceleration of tracer particles under the action of the external forcing.
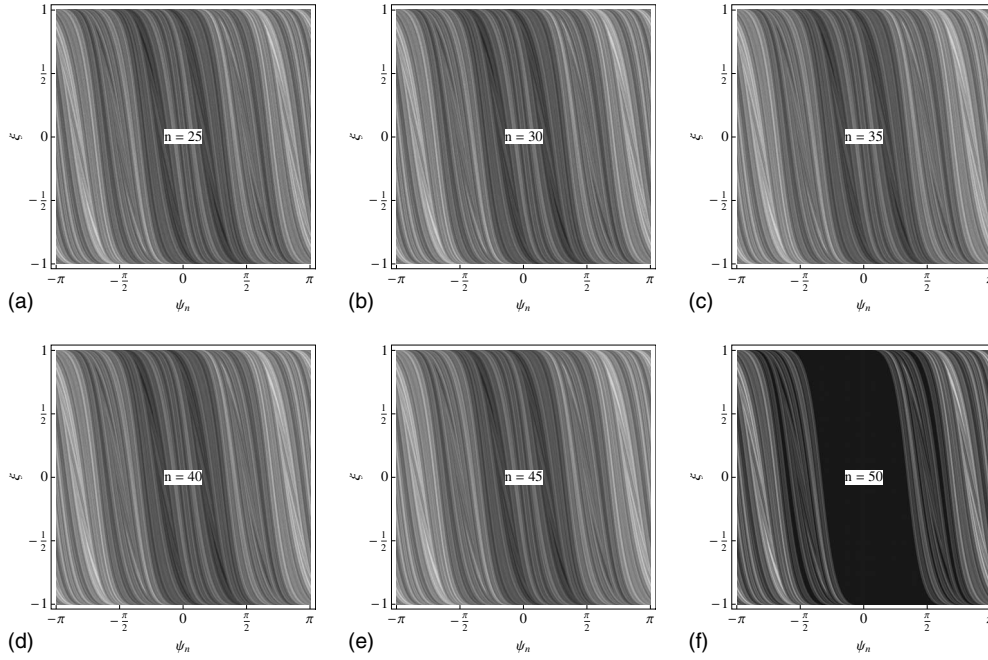
FIG. 6. Nonequilibrium phase-space densities of the open Galton channel with a geometry similar to that shown in Fig. 1, with absorbing boundaries at $x=0$ and $x=1$, and stochastic injection of particles at $x=0$ only. The plots are histograms of the phase space attached to a given disk, computed over grids of 500×500 cells, and counting the average collision rates of many trajectories on that disk. Trajectories are computed one after the other, from their injections, here at the left boundary only, to their subsequent absorption upon their first passage to either of the left and right boundaries. The corresponding disk labels $n=25,\ldots,50$ are indicated in the respective figures. Disk 50 is the one before last. Black areas correspond to absorption at the nearby boundary. The color white is associated to injection from the left boundary. Thus hues of gray correspond to phase-space regions with mixtures of phase-space points which are mapped backward to the left and right borders. The corresponding overall densities are shown in Fig. 5.

III. FORCED MULTIBAKER MAP

A time-reversible volume-preserving deterministic process can be associated to Eq. (22) in the form of a multibaker map with energy defined on the phase space $(n,[0,l_n] \times [0,l_n])_{n \in \mathbb{Z}}$, where each unit cell has area $l_n^2 \equiv a_n l^2$, $a_n = \sqrt{[1+(2n)/(2n_0+1)]}$, and the dynamics is defined according to

$$
B:(n,x,y) \mapsto
\begin{cases}
\left(n-1, \dfrac{l_{n-1}}{l_n} \dfrac{x}{s_n^-}, \dfrac{l_{n-1}}{l_n} s_{n-1}^+ y \right), & 0 \le x \le l_n s_n^- \\[3ex]
\left(n, \dfrac{x - s_n^- l_n}{s_n^0}, s_n^+ l_n + s_n^0 y \right), & l_n s_n^- \le x \le l_n (1 - s_n^+) \\[3ex]
\left(n+1, \dfrac{l_{n+1}}{l_n} \dfrac{x - s_n^- l_n - s_n^0 l_n}{s_n^+}, \dfrac{l_{n+1}}{l_n} (s_{n+1}^+ l_n + s_{n+1}^0 l_n + s_{n+1}^- y) \right), & l_n (1 - s_n^+) \le x \le l_n.
\end{cases}
\tag{39}
$$

This map has two important properties. First, the areas of the unit cells are chosen to vary with the amplitude of the velocity, which ensures that the Jacobian of B, $\frac{a_{n-1} s_{n-1}^+}{a_n s_n^-}$, or $\frac{a_{n+1} s_{n+1}^-}{a_n s_n^+}$ is unity. Second, B is time-reversal symmetric under the operator $S:(n,x,y) \to (n,l_n-y,l_n-x)$, i.e., $S \circ B = B^{-1} \circ S$, as is easily checked (Fig. 7).

Multibaker maps with energy have been considered earlier [21,22]. Here, in contrast to these references, we intro-

duce n-dependent rates $s_n^\pm$ and s_n^0 [Eq. (25)]. We will assume $D_0 = 1/2$ in the sequel so that, provided $n_0 + n \gg 1/2$, we can write

$$
s_n^\pm = \frac{1}{2} \pm \frac{1}{4} \frac{1}{2(n_0+n)+1} - \frac{1}{16} \frac{1}{[2(n_0+n)+1]^2} + \cdots.
\tag{40}
$$

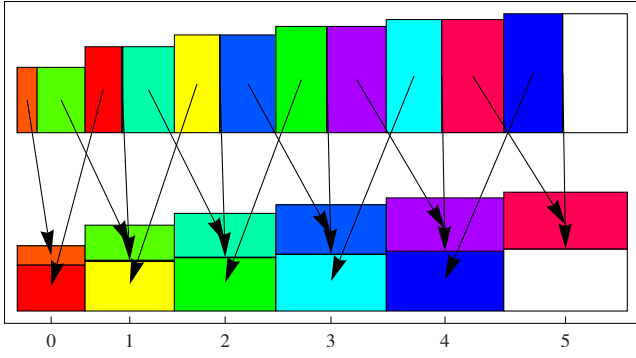Thus $s_n^0 = 1 - s_n^+ - s_n^-$ is approximated by

FIG. 7. (Color online) Forced multibaker map [Eq. (39)]. The cells have areas $a_n l^2$, with coordinates (x, y), and labeled by a positive integer n ($n_0 = 0$ here). The map divides each cell into three vertical rectangles. The left rectangle is mapped to the bottom horizontal rectangle in the left neighboring cell. Likewise the right rectangle is mapped to the top horizontal rectangle in the right neighboring cell. The middle vertical rectangle is mapped to the middle horizontal rectangle in the same cell but are so tiny they are barely visible already for $n = 1$.

$$s_n^0 = \frac{1}{8} \frac{1}{[2(n_0 + n) + 1]^2} + \cdots, \qquad (41)$$

which is vanishingly small. Therefore, when $n + n_0$ is large, the dynamics of B reduces to that of the usual multibaker map, at the exception of the energy dependence which fixes the local time scales.

A. Statistical ensembles

An initial density of points $\Gamma = (n, x, y)$, $\rho(\Gamma, 0)$, evolves under repeated iterations of B according to the action of the Frobenius-Perron operator, which, since B preserves phase-space volumes, is simply given by $\rho(\Gamma, k+1) = \rho(B^{-1}\Gamma, k)$. In order to characterize the stationary density, $\rho(\Gamma) = \lim_{k\to\infty} \rho(\Gamma, k)$, we consider the cumulative function $\mu_n(x, y, k) = \int_0^x dx' \int_0^y dy' \rho(n, x', y', k)$. Notice that ρ here refers to the statistics of the return map and therefore differs from the density ρ associated to the Galton board [Eq. (37)] by a factor proportional to the local time scale.

As shown in Appendix B, the nonequilibrium steady state of the map [Eq. (39)] associated to flux boundary conditions can be written under the form, $0 \leq x, y \leq 1$,

$$\mu_n(x l_n, y l_n) = x y \mu_n + \alpha x F_n(y), \qquad (42)$$

where F_n are generalized Takagi functions [see Eq. (B5)] [30], which, away from the boundaries where we have $F_0(y) = 0$ and $F_{N+1}(y) = 0$, are nowhere differentiable continuous functions, and α is a prefactor independent of n,

$$\alpha \to \frac{l}{2\sqrt{E}} \frac{P_+ - P_-}{\sqrt{E+L} - \sqrt{E}}, \qquad (43)$$

where the limit holds when $l \to 0$ in the continuum limit. Notice that the prefactor is proportional to l. Thus α is a small parameter in that limit.

B. Entropy and entropy production

We proceed along the lines of [31,32] to obtain expressions of the entropies and entropy production rates associated to coarse grained sets such as defined in Eq. (B16). As described in [20], the idea is that, owing to the singularity of the invariant density, the entropy should be defined with respect to a grid of phase space or partition, $\mathbb{G} = \{d\Gamma_j\}$, into small volume elements $d\Gamma_j$, and a time-dependent state $\mu_n(d\Gamma_j, t)$. The entropy associated to cell $\mathbb{C}_n$, coarse grained with respect to that grid, is defined according to

$$S_{\mathbb{G}}^t(\mathbb{C}_n) = -\sum_j \mu_n(d\Gamma_j, t) \left[\ln \frac{\mu_n(d\Gamma_j, t)}{d\Gamma_j} - 1 \right]. \qquad (44)$$

This entropy changes in a time interval τ according to

$$\begin{aligned} \Delta^\tau S^t(\mathbb{C}_n) &= S_{\mathbb{G}}^t(\mathbb{C}_n) - S_{\mathbb{G}}^{t-\tau}(\mathbb{C}_n) \\ &= S_{\{d\Gamma_j\}}^t(\mathbb{C}_n) - S_{\{\Phi^\tau d\Gamma_j\}}^t(\Phi^\tau \mathbb{C}_n), \end{aligned} \qquad (45)$$

where, in the second line, the collection of partition elements $\{d\Gamma_j\}$ was mapped to $\{\Phi^\tau d\Gamma_j\}$, which forms a partition $\Phi^\tau \mathbb{G}$ whose elements are typically stretched along the unstable foliations and folded along the stable foliations.

Following [33] and in a way analogous to the phenomenological approach to entropy production [34], the rate of entropy production at $\mathbb{C}_n$ measured with respect to the partition $\mathbb{G}$ is obtained from the entropy change [Eq. (45)] as

$$\Delta_i^\tau S_{\mathbb{G}}^t(\mathbb{C}_n) = S_{\{d\Gamma_j\}}^t(\mathbb{C}_n) - S_{\{\Phi^\tau d\Gamma_j\}}^t(\mathbb{C}_n). \qquad (46)$$

This formula is equally valid in the nonequilibrium stationary state.

As described in Appendix C, the k-entropy decreases linearly with the resolution parameter k,

$$S_k(\mathbb{C}_n) \simeq -\mu_n(\ln \mu_n - 1) - \frac{\alpha^2}{2\mu_n} k. \qquad (47)$$

Substituting this expression into Eq. (46), the k-entropy production rate is here

$$\begin{aligned} \Delta_i^\tau S_k(\mathbb{C}_n) &= \frac{1}{\tau}[S_k(\mathbb{C}_n) - S_{k+1}(\mathbb{C}_n)] \\ &= \frac{\alpha^2}{2\tau\mu_n}. \end{aligned} \qquad (48)$$

Using Eqs. (10), (26), and (43), it is readily checked that this expression yields the phenomenological entropy production rate [Eq. (17)] $\Delta_i^\tau S_k(\mathbb{C}_n) \xrightarrow{\tau, l \to 0} d_i S(X = nl)/dt$.

IV. CONCLUSIONS

In this paper, we have considered the influence of an external field on a class of time-reversible deterministic volume-preserving models of diffusive systems known as Galton boards or, equivalently, forced periodic two-dimensional Lorentz gases.

Though the particles are accelerated as they move along the direction of the external field, the motion is recurrent in
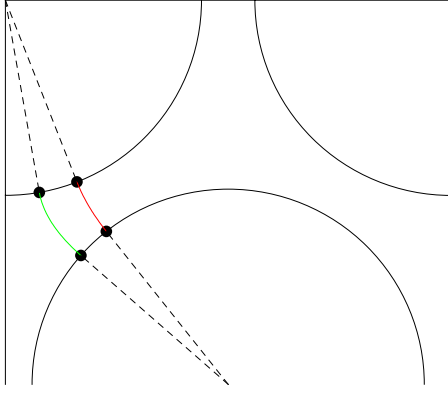
FIG. 8. (Color online) The external field induces a bifurcation such that the simple periodic orbit bouncing off two neighboring disks at normal angles is replaced by two such orbits. In this situation where $E=0$, which corresponds to a vanishing kinetic energy on the left border, one of these two periodic orbits is stable (to the left) and the other one unstable (to the right). The stability of the periodic orbit is quickly lost as E is increased.

the absence of a dissipative mechanism, which is to say that tracer particles keep coming back to the region of near zero velocity. In other words, particles do not drift in the direction of the external field. Rather, forced periodic Lorentz gases remain purely diffusive in two dimensions, albeit with a velocity-dependent diffusion coefficient. Consequently, the scaling laws relating time and displacement are different from that of a homogeneously diffusive system. The macroscopic description through a Fokker-Planck equation is however unchanged since the mobility coefficient vanishes identically in dimension 2.

It will be interesting to investigate the behavior of three-dimensional periodic Lorentz gases in a uniform external field. As our analysis showed, the mobility does not vanish in dimension three so that the Fokker-Planck equation retains a drift term. Being inversely proportional to the tracers' velocity amplitudes, this drift decreases with increasing kinetic energy. A crossover is thus expected between biased and diffusive motions.

As far as their statistical properties are concerned, Galton boards are essentially identical to the field-free periodic two-dimensional Lorentz gases. A closed system with reflecting boundaries relaxes to an equilibrium state with a uniform invariant measure. This is to say that tracers spend equal amounts of time in all parts of the system. Open systems with absorbing boundaries yield nonequilibrium states. Given constant rates of tracer injection at the borders, the system reaches a nonequilibrium stationary state which is characterized by a fractal invariant measure.

The fractality of the invariant measure associated to the nonequilibrium state of such a system was established analytically for a multibaker map describing the motion of random walkers accelerated by a uniform external field. The computation of the coarse-grained entropies associated to arbitrarily refined partitions yields expressions which depart from their local equilibrium expressions by a term which decreases linearly with the logarithm of the number of elements in the partition. This term is responsible for the positiveness of the entropy production rate with a value consistent with the phenomenological expression of thermodynamics.

APPENDIX A: ELLIPTIC ISLANDS

In this appendix, we discuss the possible lack of ergodicity of the Galton board. This situation occurs when the system admits periodic orbits whose kinetic energy remains
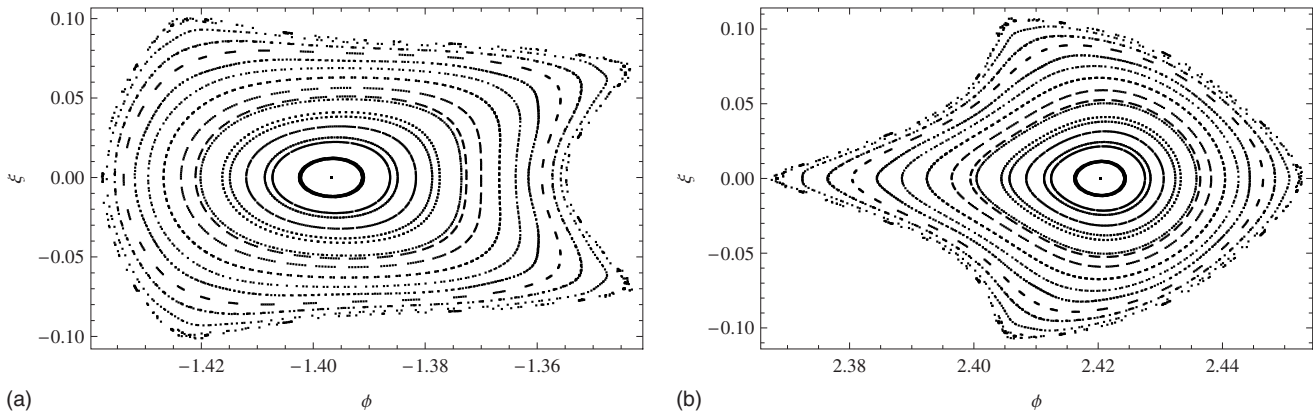

FIG. 9. Elliptic islands around the stable periodic orbit shown in Fig. 8: (a) disk on the upper left corner; (b) central disk. The phase-space coordinates used here (not the appropriate Birkhoff coordinates) are ϕ, the angle around the corresponding disk, and ξ the sinus of the velocity angle measures with respect to the normal to the disk.

small, in which case the external field is able to stabilize them. Figure 8 shows such an example. In this case, elliptic islands coexist with chaotic trajectories, as seen in Fig. 9.

We notice that a mixed phase space is typically expected in Hamiltonian chaotic systems—as is the case, e.g., with the sine-circle map. This is an undesirable feature for our own sake. However the elliptic islands disappear if the energy value E is large enough. We observe from our numerical computations that $E = l/2$ is already large enough.

In particular, letting $y = l_n$, we recover

$$\mu_n(l_n, l_n, k+1) = s_{n+1}^- \mu_{n+1}(l_{n+1}, l_{n+1}, k) + s_n^0 \mu_n(l_n, l_n, k) + s_{n-1}^+ \mu_{n-1}(l_{n-1}, l_{n-1}, k), \quad \text{(B2)}$$

which is identical to Eq. (22) with $\mu_n(k) \equiv \mu_n(l_n, l_n, k)$. Let μ_n denote the steady state of this equation, $\mu_n = \lim_{k \to \infty} \mu_n(l_n, l_n, k)$.

The steady state of Eq. (B1) can be written under the form, $0 \le x, y \le 1$,

$$\mu_n(x l_n, y l_n) \equiv \lim_{k \to \infty} \mu_n(x l_n, y l_n, k)$$
$$= xy\mu_n + 2x(s_{n+1}^- \mu_{n+1} - s_n^+ \mu_n) F_n(y)$$
$$\equiv xy\mu_n + \alpha x F_n(y), \quad \text{(B3)}$$

where we introduced the generalized Takagi functions F_n, with a prefactor, $\alpha = 2(s_{n+1}^- \mu_{n+1} - s_n^+ \mu_n)$, which, as in Eqs. (27)–(29) is easily seen to be independent of n:

$$2(s_{n+1}^- \mu_{n+1} - s_n^+ \mu_n) = \sqrt{\frac{2(n_0 + n + 1)}{2n_0 + 1}} (P_{n+1} - P_n),$$
$$= \sqrt{\frac{2}{2n_0 + 1}} \frac{P_+ - P_-}{H_{N+n_0}^{1/2} - H_{n_0}^{1/2}}. \quad \text{(B4)}$$

In the limit $l \to 0$, we recover Eq. (43).

Substituting Eq. (B3) into Eq. (B1), the generalized Takagi function F is found to satisfy a functional equation of the de Rham type [36]

APPENDIX B: NONEQUILIBRIUM STATIONARY STATE OF THE FORCED MULTIBAKER MAP

The identification of the nonequilibrium stationary state of the force multibaker map [Eq. (39)] proceeds along the lines of Refs. [23,32,35]. Under the assumption that the x dependence of the initial density is trivial, we can write $\mu_n(x, y, k) = x/l_n \mu_n(l_n, y, k)$. Letting $0 \le y \le 1$, it is then easy to verify that $\mu_n(l_n, y l_n, k)$ obeys the functional equation

$$\mu_n(l_n, y l_n, k+1) = \begin{cases} s_{n+1}^- \mu_{n+1}\left(l_{n+1}, \dfrac{y}{s_n^+} l_{n+1}, k\right), & 0 \le y \le s_n^+ \\[3mm] s_{n+1}^- \mu_{n+1}(l_{n+1}, l_{n+1}, k) + s_n^0 \mu_n\left(l_n, \dfrac{y - s_n^+}{s_n^0} l_n, k\right), & s_n^+ \le y \le 1 - s_n^- \\[3mm] s_{n+1}^- \mu_{n+1}(l_{n+1}, l_{n+1}, k) + s_n^0 \mu_n(l_n, l_n, k) + s_{n-1}^+ \mu_{n-1}\left(l_{n-1}, \dfrac{y - s_n^+ - s_n^0}{s_n^-} l_{n-1}, k\right), & (1 - s_n^-) \le y \le 1. \end{cases} \quad \text{(B1)}$$

$$F_n(y) = \begin{cases} \dfrac{y}{2s_n^+} + s_{n+1}^- F_{n+1}\left(\dfrac{y}{s_n^+}\right), & 0 \le y < s_n^+ \\[3mm] \dfrac{1}{2} + s_n^0 F_n\left(\dfrac{y - s_n^+}{s_n^0}\right), & s_n^+ \le y < 1 - s_n^- \\[3mm] \dfrac{1 - y}{2s_n^-} + s_{n-1}^+ F_{n-1}\left(\dfrac{y - s_n^+ - s_n^0}{s_n^-}\right), & 1 - s_n^- < y \le 1. \end{cases} \quad \text{(B5)}$$

The boundary conditions are such that the density is uniform at $n = 0, N+1$, implying $F_0(y) = F_{N+1}(y) = 0$. Notice that this function reduces to the Takagi function in the limit $n, N \to \infty$, $n \ll N$. Indeed $s_\infty^-, s_\infty^+ = 1/2$, $s_\infty^0 = 0$. Therefore Eq. (B3) is similar to the corresponding expression obtained for the multibaker map, see [20].

1. Generalized Takagi functions

For the sake of plotting $F_n(y)$, it is convenient to consider the graph of $F_n(y)$ vs y as parametrized by a real variable, $0 \le x \le 1$, defined so that

$$y_n(x) = \begin{cases} s_n^+ y_{n+1}(3x), & 0 \le x < 1/3 \\ s_n^+ + s_n^0 y_n(3x - 1), & 1/3 \le x < 2/3 \\ s_n^+ + s_n^0 + s_n^- y_{n-1}(3x - 2), & 2/3 \le x < 1 \end{cases}$$
$$\text{(B6)}$$

and

$$F_n(x) = \begin{cases} \dfrac{y_n(x)}{2s_n^+} + s_{n+1}^- F_{n+1}(3x), & 0 \leq x < 1/3 \\[3mm] \dfrac{1}{2} + s_n^0 F_n(3x-1), & 1/3 \leq y < 2/3 \\[3mm] \dfrac{1-y_n(x)}{2s_n^-} + s_{n-1}^+ F_{n-1}(3x-2), & 2/3 \leq y < 1. \end{cases}$$

$$(B7)$$

The boundary conditions are taken so that $y_n(x)=y_1(x)$, $n < 1$, and $y_n(x)=y_N(x)$, $n > N$. As above, $F_n(x)=0$, $n<1$, or $n>N$.

Starting from the end points $y(n,0)=0$, $y(n,1)=1$, and $F_n(0)=F_n(1)=0$, $1 \leq n \leq N$, we successively compute $y_n(x_k)$ and $F_n(x_k)$, $1 \leq n \leq N$ at points $x_k = \Sigma_{j=1}^{k} 3^{-j}\omega_j$, where, for every $k \geq 1$, there are 3^k different sequences $\{\omega_1, \ldots, \omega_k\}$, $\omega_j \in \{0,1,2\}$, $1 \leq j \leq k$.

The graphs of $F_n(x_k)$ vs $y_n(x_k)$ are displayed in Fig. 10 for a chain of $N=100$ sites and $k=8$ and compared to the corresponding graphs of the incomplete Takagi functions [23], which can be obtained from Eq. (B7) by setting $s_n^+ = s_n^- \equiv 1/2$ and $s_n^0 = 0$,

$$y(x) = \begin{cases} \dfrac{1}{2}y(3x), & 0 \leq x < 1/3 \\[3mm] \dfrac{1}{2}, & 1/3 \leq x < 2/3 \\[3mm] \dfrac{1}{2} + \dfrac{1}{2}y(3x-2), & 2/3 \leq x < 1 \end{cases}$$

$$(B8)$$

and

$$T_n(x) = \begin{cases} y(x) + \dfrac{1}{2}T_{n+1}(3x), & 0 \leq x < 1/3 \\[3mm] \dfrac{1}{2}, & 1/3 \leq y < 2/3 \\[3mm] 1 - y(x) + \dfrac{1}{2}T_{n-1}(3x-2), & 2/3 \leq y < 1. \end{cases}$$

$$(B9)$$

In passing, we note that, on the one hand, Eq. (B8) is a functional equation whose solution is the Cantor function. On the other hand, the triadic representation of the incomplete Takagi functions [Eq. (B9)] is many to one. Their graphs, $T_n(x)$ vs $y(x)$, are nevertheless identical to those obtained using the usual representation of the incomplete Takagi functions.

2. Symbolic dynamics

By substituting the triadic expansion of x in Eqs. (B6) and (B7), $x(\{\omega_0, \ldots, \omega_k\}) = \Sigma_{j=0}^{k} \omega_j 3^{-(j+1)}$, $\omega_j \in \{0,1,2\}$, we
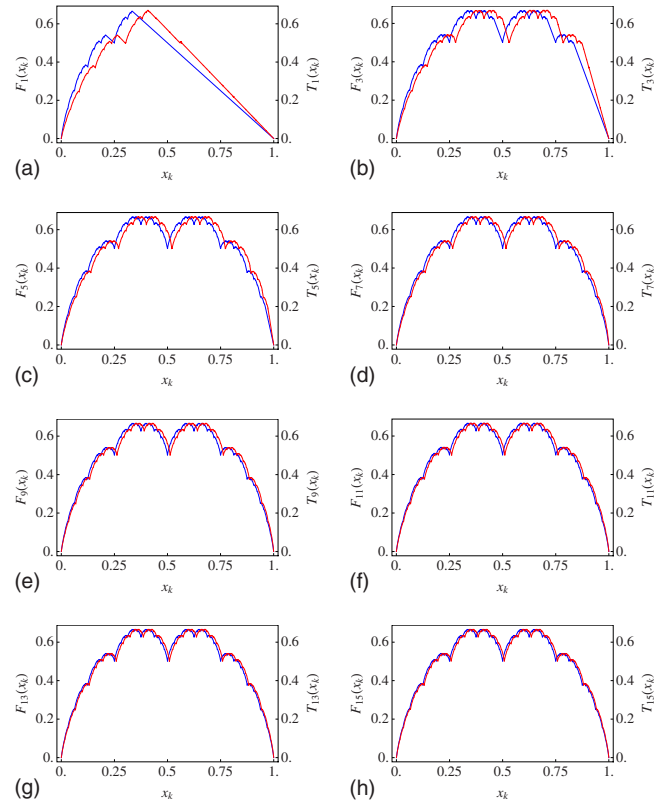

FIG. 10. (Color online) Comparison between the graphs of $F_n(x_k)$ vs $y_n(x_k)$ (red and slightly shifted to the right) and the corresponding incomplete Takagi functions $T_n(x_k)$ (blue). Each curve is computed at $3^{10}+1$ different points x, uniformly spread between 0 and 1. Only $2^{10}+1$ correspond to different points in the graphs of T_n.

obtain the following symbolic representations of points y in cell n:

$$y_n(\{\omega_0, \ldots, \omega_k\}) = \begin{cases} s_n^+ y_{n+1}(\{\omega_1, \ldots, \omega_k\}), & \omega_0 = 0 \\[2mm] s_n^+ + s_n^0 y_n(\{\omega_1, \ldots, \omega_k\}), & \omega_0 = 1 \\[2mm] s_n^+ + s_n^0 + s_n^- y_{n-1}(\{\omega_1, \ldots, \omega_k\}), & \omega_0 = 2. \end{cases}$$

$$(B10)$$

Starting from

$$y_n(\{\omega_0\}) = \begin{cases} 0, & \omega_0 = 0 \\[2mm] s_n^+, & \omega_0 = 1 \\[2mm] s_n^+ + s_n^0, & \omega_0 = 2, \end{cases}$$

$$(B11)$$

we can write

$$y_n(\{\omega_0, \ldots, \omega_k\}) = y_n(\{\omega_0\}) + s_n^{1-\omega_0} y_{n+1-\omega_0}(\{\omega_1, \ldots, \omega_k\})$$

$$= y_n(\{\omega_0\}) + s_n^{1-\omega_0} y_{n+1-\omega_0}(\{\omega_1\}) + s_n^{1-\omega_0} s_{n+1-\omega_0}^{1-\omega_1} y_{n+2-\omega_0-\omega_1}(\{\omega_2, \ldots, \omega_k\})$$

$$\vdots$$

$$= \sum_{i=0}^{k} \left[\prod_{j=0}^{i-1} s_{n+j-\omega_0-\ldots-\omega_{j-1}}^{1-\omega_j} \right] y_{n+i-\omega_0-\ldots-\omega_{i-1}}(\{\omega_i\}). \tag{B12}$$

Substituting this symbolic dynamics into the expression of F_n [Eq. (B5)] we write

$$F_n(\{\omega_0, \ldots, \omega_k\}) = \begin{cases} \dfrac{1}{2} y_{n+1}(\{\omega_1, \ldots, \omega_k\}) + s_{n+1}^- F_{n+1}(\{\omega_1, \ldots, \omega_k\}), & \omega_0 = 0 \\[2mm] 1/2 + s_n^0 F_n(\{\omega_1, \ldots, \omega_k\}), & \omega_0 = 1 \\[2mm] \dfrac{1}{2}(1 - y_{n-1}(\{\omega_1, \ldots, \omega_k\})) + s_{n-1}^+ F_{n-1}(\{\omega_1, \ldots, \omega_k\}), & \omega_0 = 2. \end{cases} \tag{B13}$$

Let $\Delta y_n(\omega_0, \ldots, \omega_k)$ denote the height of a horizontal cylinder set of the unit square coded by the sequence $\{\omega_0, \ldots, \omega_k\}$. We have

$$\Delta y_n(\omega_0, \ldots, \omega_k) \equiv y_n(\{\omega_0, \ldots, \omega_k + 1\}) - y_n(\{\omega_0, \ldots, \omega_k\}), \tag{B14}$$

where the notation $y_n(\{\omega_0, \ldots, \omega_k + 1\})$ is literal whenever $\omega_k \neq 2$. Otherwise $y_n(\{\omega_0, \ldots, \omega_{k-1}, 2+1\}) \equiv y_n(\{\omega_0, \ldots, \omega_{k-1} + 1, 0\})$, and we set $y_n(\{2, \ldots, 2, 2+1\}) \equiv 1$. We have the following identities

$$\begin{aligned} \Delta y_n(0, \omega_1, \ldots, \omega_k) &= s_n^+ \Delta y_{n+1}(\omega_1, \ldots, \omega_k) \\ \Delta y_n(1, \omega_1, \ldots, \omega_k) &= s_n^0 \Delta y_n(\omega_1, \ldots, \omega_k) \\ \Delta y_n(2, \omega_1, \ldots, \omega_k) &= s_n^- \Delta y_{n-1}(\omega_1, \ldots, \omega_k). \end{aligned} \tag{B15}$$

Therefore

$$\Delta y_n(\omega_0, \ldots, \omega_k) = \prod_{i=0}^{k} s_{n+i-\omega_0-\ldots-\omega_{i-1}}^{1-\omega_i}, \tag{B16}$$

which is nothing but the probability associated to the trajectory starting at position n and coded by the sequence $\{\omega_0, \ldots, \omega_k\}$.

Likewise, the measure of the cylinder set $\Delta y_n(\omega_0, \ldots, \omega_k)$ is

$$\begin{aligned} \Delta \mu_n(\omega_0, \ldots, \omega_k) &\equiv \mu_n\{y_n[(\omega_0, \ldots, \omega_{k-1} + 1)]\} \\ &\quad - \mu_n\{y_n[(\omega_0, \ldots, \omega_{k-1})]\} \\ &= \mu_n \Delta y_n(\omega_0, \ldots, \omega_k) + \alpha \Delta F_n(\omega_0, \ldots, \omega_k), \end{aligned} \tag{B17}$$

and we have the following set of identities for ΔF_n:

$$\begin{aligned} \Delta F_n(0, \omega_1, \ldots, \omega_k) &= \frac{1}{2} \Delta y_{n+1}(\omega_1, \ldots, \omega_k) + s_{n+1}^- \Delta F_{n+1}(\omega_1, \ldots, \omega_k) \\ \Delta F_n(1, \omega_1, \ldots, \omega_k) &= s_n^0 \Delta F_n(\omega_1, \ldots, \omega_k) \\ \Delta F_n(2, \omega_1, \ldots, \omega_k) &= -\frac{1}{2} \Delta y_{n-1}(\omega_1, \ldots, \omega_k) + s_{n-1}^+ \Delta F_{n-1}(\omega_1, \ldots, \omega_k). \end{aligned} \tag{B18}$$

That is,

$$\Delta F_n(\omega_0, \ldots, \omega_k) = \frac{1}{2}(1 - \omega_0) \Delta y_{n+1-\omega_0}(\omega_1, \ldots, \omega_k) + s_{n+1-\omega_0}^{\omega_0-1} \Delta F_{n+1-\omega_0}(\omega_1, \ldots, \omega_k). \tag{B19}$$

Notice that it is possible to solve this system recursively, starting from

$$\Delta F_n(\omega_0) = \begin{cases} 1/2, & \omega_0 = 0 \\ 0, & \omega_0 = 1 \\ -1/2, & \omega_0 = 2. \end{cases} \qquad \text{(B20)}$$

We thus have a complete characterization of the nonequilibrium stationary state of B [Eq. (39)] associated to flux boundary conditions.

APPENDIX C: *k*-ENTROPY

Given a phase-space partition into the 3^k cylinder sets coded by the sequences $\underline{\omega}_k \equiv \{\omega_0, \dots, \omega_{k-1}\}$, $\omega_i \in \{0, 1, 2\}$, as described in Appendix B, the k-entropy of the stationary state Eq. (42) relative to the volume measure of cell n is defined by

$$S_k(\mathbb{C}_n) = -\sum_{\underline{\omega}_k} \Delta\mu_n(\underline{\omega}_k) \left[\ln \frac{\Delta\mu_n(\underline{\omega}_k)}{\Delta y_n(\underline{\omega}_k)} - 1 \right]. \qquad \text{(C1)}$$

By summing over the first digit, it follows immediately from Eqs. (B1) and (B16) that the k-entropy verifies a recursion relation,

$$S_k(\mathbb{C}_n) = -s_{n+1}^- \rho_{n+1} \ln \frac{s_{n+1}^-}{s_n^+} - s_{n-1}^+ \rho_{n-1} \ln \frac{s_{n-1}^+}{s_n^-} + s_{n+1}^- S_{k-1}(\mathbb{C}_{n+1})$$
$$+ s_n^0 S_{k-1}(\mathbb{C}_n) + s_{n-1}^+ S_{k-1}(\mathbb{C}_{n-1}), \qquad \text{(C2)}$$

with the $k=0$-entropy given by

$$S_0(\mathbb{C}_n) = -\mu_n \ln \mu_n \qquad \text{(C3)}$$

and boundary conditions

$$\begin{aligned} S_k(\mathbb{C}_0) &= -\rho_- \ln \rho_- \\ S_k(\mathbb{C}_{N+1}) &= -\rho_+ \ln \rho_+. \end{aligned} \qquad \text{(C4)}$$

The k-entropy can be computed based on the above recursion relation. However, in order to obtain the dependence of the entropy on the resolution parameter k, it is more useful to consider the expansion of Eq. (C1) in powers of ρ_n. Let us denote by $\underline{\omega}_k$ the sequence $\{\omega_0, \dots, \omega_{k-1}\}$

$$S_k(\mathbb{C}_n) = -\mu_n \sum_{\underline{\omega}_k} \Delta y_n(\underline{\omega}_k) \left[1 + \frac{\alpha}{\mu_n} \frac{\Delta F_n(\underline{\omega}_k)}{\Delta y_n(\underline{\omega}_k)} \right]$$
$$\times \left\{ \ln \mu_n \left[1 + \frac{\alpha}{\mu_n} \frac{\Delta F_n(\underline{\omega}_k)}{l \Delta y_n(\underline{\omega}_k)} \right] - 1 \right\}$$
$$= -\mu_n(\ln \mu_n - 1) - \alpha(\ln \mu_n - 1) \sum_{\underline{\omega}_k} \Delta F_n(\underline{\omega}_k)$$

$$- \frac{\alpha^2}{2\mu_n} \sum_{\underline{\omega}_k} \frac{[\Delta F_n(\underline{\omega}_k)]^2}{\Delta y_n(\underline{\omega}_k)} + \mathcal{O}(\alpha)^3. \qquad \text{(C5)}$$

The second term on the right-hand side (rhs) of this equation vanishes since

$$\sum_{\underline{\omega}_k} \Delta F_n(\underline{\omega}_k) = 0. \qquad \text{(C6)}$$

As of the third term on the rhs of Eq. (C5), proportional to α^2, we have, using Eqs. (B15) and (B18),

$$\begin{aligned} \Delta_n^2(k) &\equiv \sum_{\underline{\omega}_k} \frac{[\Delta F_n(\underline{\omega}_k)]^2}{\Delta y_n(\underline{\omega}_k)} \\ &= \frac{1}{4s_n^+} + \frac{1}{4s_n^-} + \frac{(s_{n+1}^-)^2}{s_n^+} \Delta_{n+1}^2(k-1) + s_n^0 \Delta_n^2(k-1) \\ &\quad + \frac{(s_{n-1}^+)^2}{s_n^-} \Delta_{n-1}^2(k-1) \\ &= \frac{1}{4s_n^+} + \frac{1}{4s_n^-} + \sum_{\eta=0}^{2} \frac{(s_{n+1-\eta}^{\eta-1})^2}{s_n^{1-\eta}} \Delta_{n+1-\eta}^2(k-1) \end{aligned} \qquad \text{(C7)}$$

$$= \sum_{i=0}^{k-1} \sum_{\eta_1, \dots, \eta_{i-1}} \left[\prod_{j=1}^{i} \frac{(s_{n+j-\eta_1-\dots-\eta_j}^{\eta_j-1})^2}{s_{n+j-1-\eta_1-\dots-\eta_{j-1}}^{1-\eta_j}} \right]$$
$$\times \left(\frac{1}{4s_{n+i-\eta_1-\dots-\eta_i}^+} + \frac{1}{4s_{n+i-\eta_1-\dots-\eta_i}^-} \right). \qquad \text{(C8)}$$

Substituting the expressions of the probability transitions from Eqs. (40) and (41), Eq. (C8) is found to be

$$\begin{aligned} \Delta_n^2(k) &= \sum_{\underline{\omega}_k} \frac{[\Delta F_n(\underline{\omega}_k)]^2}{\Delta y_n(\underline{\omega}_k)} \\ &= k + \frac{12k^2 - 9k}{32(n+n_0)^2} + \mathcal{O}(n+n_0)^{-4}. \end{aligned} \qquad \text{(C9)}$$

The first term on the rhs of this expression, which is the only term that survives in the continuum limit where $n+n_0 \gg 1$, is responsible for the linear decay of the k-entropy [Eq. (47)].

[1] P. Gaspard, *Chaos, Scattering, and Statistical Mechanics* (Cambridge University Press, Cambridge, 1998).

[2] F. Galton, *Natural Inheritance* (Macmillan, London, 1889).

[3] M. Barile and E. W. Weisstein, *Galton Board*, From MathWorld: A Wolfram Web Resource. http:// mathworld.wolfram.com/GaltonBoard.html

[4] N. Chernov and D. Dolgopyat, Phys. Rev. Lett. **99**, 030601 (2007).

[5] N. Chernov and D. Dolgopyat, J. Am. Math. Soc. **22**, 821 (2009).

[6] P. L. Krapivsky and S. Redner, Phys. Rev. E **56**, 3822 (1997).

[7] J. Piasecki and E. Wajnryb, J. Stat. Phys. **21**, 549 (1979).

[8] H. A. Lorentz, Proc. R. Acad. Sci. Amsterdam **7**, 438 (1905).

[9] H. van Beijeren, Rev. Mod. Phys. **54**, 195 (1982).

[10] C. P. Dettmann, in *Hard Ball Systems and Lorentz Gas: Encyclopedia of Mathematical Sciences*, edited by D. Szasz (Springer, Berlin, 2000).

[11] S. Chapman and T. G. Cowling, *The Mathematical Theory of Nonuniform Gases*, 3rd ed. (Cambridge University Press, Cambridge, England, 1970), Chap. 10.

[12] E. H. Hauge, in *Transport Phenomena*, edited by G. Kirczenow and J. Marro (Springer, Berlin, 1974).

[13] L. A. Bunimovich and Ya. G. Sinai, Commun. Math. Phys. **78**, 247 (1980); **78**, 479 (1981).

[14] W. G. Hoover, *Molecular Dynamics* (Springer-Verlag, Heidelberg, 1986).

[15] D. J. Evans and G. P. Morriss, *Statistical Mechanics of Nonequilibrium Liquids*, 2nd ed. (Cambridge University Press, Cambridge, England, 2008).

[16] B. Moran and W. Hoover, J. Stat. Phys. **48**, 709 (1987).

[17] N. I. Chernov, G. L. Eyink, J. L. Lebowitz, and Ya. G. Sinai, Phys. Rev. Lett. **70**, 2209 (1993); Commun. Math. Phys. **154**, 569 (1993).

[18] P. Drude, Ann. Phys. **306**, 566 (1900); **308**, 369 (1900).

[19] N. W. Ashcroft and N. D. Mermin, *Solid State Physics* (Brooks-Cole, Belmont, MA, 1976).

[20] F. Barra, P. Gaspard, and T. Gilbert, Phys. Rev. E **80**, 021126 (2009).

[21] S. Tasaki and P. Gaspard, Theor. Chem. Acc. **102**, 385 (1999).

[22] S. Tasaki and P. Gaspard, J. Stat. Phys. **101**, 125 (2000).

[23] S. Tasaki and P. Gaspard, J. Stat. Phys. **81**, 935 (1995).

[24] J.-P. Tignol, *Galois' Theory of Algebraic Equations* (World Scientific, Singapore, 2001).

[25] J. Machta and R. Zwanzig, Phys. Rev. Lett. **50**, 1959 (1983).

[26] P. Gaspard, G. Nicolis, and J. R. Dorfman, Physica A **323**, 294 (2003).

[27] J. Sondow and E. W. Weisstein, Harmonic Number, From MathWorld: A Wolfram Web Resource. http://mathworld.wolfram.com/HarmonicNumber.html

[28] S. Koga, J. Phys. Soc. Jpn. **70**, 1260 (2001).

[29] P. Gaspard, Physica A **240**, 54 (1997).

[30] T. Takagi, Proc. Phys. Math. Soc. Jpn. Ser. II **1**, 176 (1903).

[31] P. Gaspard, J. Stat. Phys. **88**, 1215 (1996).

[32] T. Gilbert and J. R. Dorfman, J. Stat. Phys. **96**, 225 (1999).

[33] J. R. Dorfman, P. Gaspard, and T. Gilbert, Phys. Rev. E **66**, 026110 (2002).

[34] S. de Groot and P. Mazur, *Nonequilibrium Thermodynamics* (North-Holland, Amsterdam, 1962); *Nonequilibrium Thermodynamics* (Dover, New York, 1984) reprinted.

[35] S. Tasaki, T. Gilbert, and J. R. Dorfman, Chaos **8**, 424 (1998).

[36] G. de Rham, Enseign. Math. **3**, 71 (1957); Rend. Semin. Mat. Torino **16**, 101 (1957).